4220 *Biochemistry* **2010,** *49,* 4220–4226
DOI: 10.1021/bi100335u

BIOCHEMISTRY
including biophysical chemistry & molecular biology
Article

NMR Characterization of the Interaction of the *Salmonella* Type III Secretion System Protein SipD and Bile Salts[†,‡]

Yu Wang, Bryce A. Nordhues, Dalian Zhong, and Roberto N. De Guzman*

Department of Molecular Biosciences, The University of Kansas, 1200 Sunnyside Avenue, Lawrence, Kansas 66045

Received March 5, 2010; Revised Manuscript Received April 15, 2010

ABSTRACT: *Salmonella* and *Shigella* bacteria require the type III secretion system (T3SS) to inject virulence proteins into their hosts and initiate infections. The tip proteins SipD and IpaD are critical components of the *Salmonella* and *Shigella* T3SS, respectively. Recently, SipD and IpaD have been shown to interact with bile salts, which are enriched in the intestines, and are hypothesized to act as environmental sensors for these enteric pathogens. Bile salts activate the *Shigella* T3SS but repress the *Salmonella* T3SS, and the mechanism of this differing response to bile salts is poorly understood. Further, how SipD binds to bile salts is currently unknown. Computer modeling predicted that IpaD binds the bile salt deoxycholate in a cleft formed by the N-terminal domain and the long central coiled coil of IpaD. Here, we used NMR methods to determine which SipD residues are affected by the interaction with the bile salts deoxycholate, chenodeoxycholate, and taurodeoxcholate. The bile salts perturbed nearly the same set of SipD residues; however, the largest chemical shift perturbations occurred away from what was predicted for the bile salt binding site in IpaD. Our NMR results indicate that that bile salt interaction of SipD will be different from what was predicted for IpaD, suggesting a possible mechanism for the differing response of *Salmonella* and *Shigella* to bile salts.

The type III secretion system (T3SS)[1] is essential in the pathogenesis of many Gram-negative bacteria (*1*), and it consists of a needle apparatus, which is a nanometer-scale bacterial injector found on the bacterial surface. A structural component of the T3SS needle apparatus is the tip protein (*2*, *3*), which is known as SipD in *Salmonella typhimurium*, IpaD in *Shigella flexneri* (*3*), and BipD in *Burkholderia pseudomallei*. The tip proteins are critical in the assembly of the T3SS needle apparatus and in bacterial pathogenesis (*4*−*6*). Recently, IpaD was shown to bind the bile salts deoxycholate, taurodeoxycholate, and chenodeoxycholate (*7*), and this specific binding was suggested to function as an environmental signal to activate the T3SS in *S. flexneri* (*8*). The same study also showed that SipD binds to deoxycholate (*7*); however, other studies have shown that bile salts suppressed the invasiveness of *Salmonella* (*9*, *10*). The crystal structures of IpaD (*11*) and SipD (to be reported elsewhere) are highly similar (with C^{α} rmsd of 1.4 Å); thus it is not clear how bile salts would interact with IpaD and SipD to induce opposing effects: activation of the *Shigella* T3SS and inactivation of the *Salmonella* T3SS.

Using computer docking simulation, Stensrud et al. (*7*) predicted that deoxycholate binds IpaD in a cleft formed by the central coiled-coil and the N-terminal domain of IpaD, which was then confirmed by fluorescence spectroscopy and mutagenesis (*7*). Here, we used NMR methods to identify which SipD residues are involved in the interaction with bile salts deoxycholate, taurodeoxycholate, and chenodeoxycholate. Our NMR results indicated that bile salts bind SipD in a different site from what is predicted for IpaD, suggesting a basis for the differing mechanism of bile salt interaction observed for *Shigella* and *Salmonella*.

EXPERIMENTAL PROCEDURES

Protein Expression and Purification. The coding region for wild-type *S. typhimurium* SipD residues 39−343 was PCR amplified and subcloned into pET-21a with a His_6-tagged GB1 domain and a tobacco etch virus (TEV) protease cleavage site appended at the N-terminus of $SipD^{39-343}$ (after cleavage of the fusion tag, $SipD^{39-343}$ retained a three-residue cloning artifact "GHM" at its N-terminus). All growth media contained 30 μg/mL kanamycin and 100 μg/mL carbenicillin. For protein expression, the $SipD^{39-343}$ expression plasmid was transformed into *Escherichia coli* BL21(DE3) DNAY, and a starter culture was grown at 37 °C overnight in 20 mL of LB medium followed by centrifugation. Perdeuterated ^{15}N,^{13}C-labeled $SipD^{39-343}$ was obtained by resuspending the starter culture in 1 L of M9 minimal media dissolved in 99% D_2O (Cambridge Isotopes) and supplemented with 2 g/L [^{13}C]glucose (Isotec) and 1 g/L [^{15}N]ammonium chloride (Isotec). Isotopically ^{15}N-labeled $SipD^{39-343}$ was obtained by resuspending the starter culture in 1 L of M9 minimal medium supplemented with 1 g/L [^{15}N]ammonium chloride. Cells were grown at 37 °C until $A_{600} \sim 0.6-0.8$, induced with 1 mM IPTG, and cell growth was continued in a 15 °C shaker incubator overnight. Cells were harvested by centrifugation, resuspended in 30 mL of binding buffer (500 mM NaCl, 20 mM Tris-HCl, 500 mM NaCl, 5 mM imidazole, pH 8.0), and stored at −20 °C. To purify $SipD^{39-343}$, cells were thawed on ice, and 40 μL of 1 mM phenylmethanesulfonyl fluoride was added before sonication.

[†]Supported by NIH Grants R01AI074856 and RR017708.
[‡]NMR assignments have been deposited in the BioMagResBank, BMRB number 16729.
*Corresponding author: e-mail, rdguzman@ku.edu; fax, (785) 864-5294; phone, (785) 864-4923.
[1]Abbreviations: CMC, critical micelle concentration; HSQC, heteronuclear single quantum coherence spectroscopy; K_d, dissociation constant; NMR, nuclear magnetic resonance spectroscopy; RMSD, root mean square deviation; TEV, tobacco etch virus; T3SS, type III secretion system; TROSY, transverse relaxation spectroscopy.

 Published on Web 04/16/2010

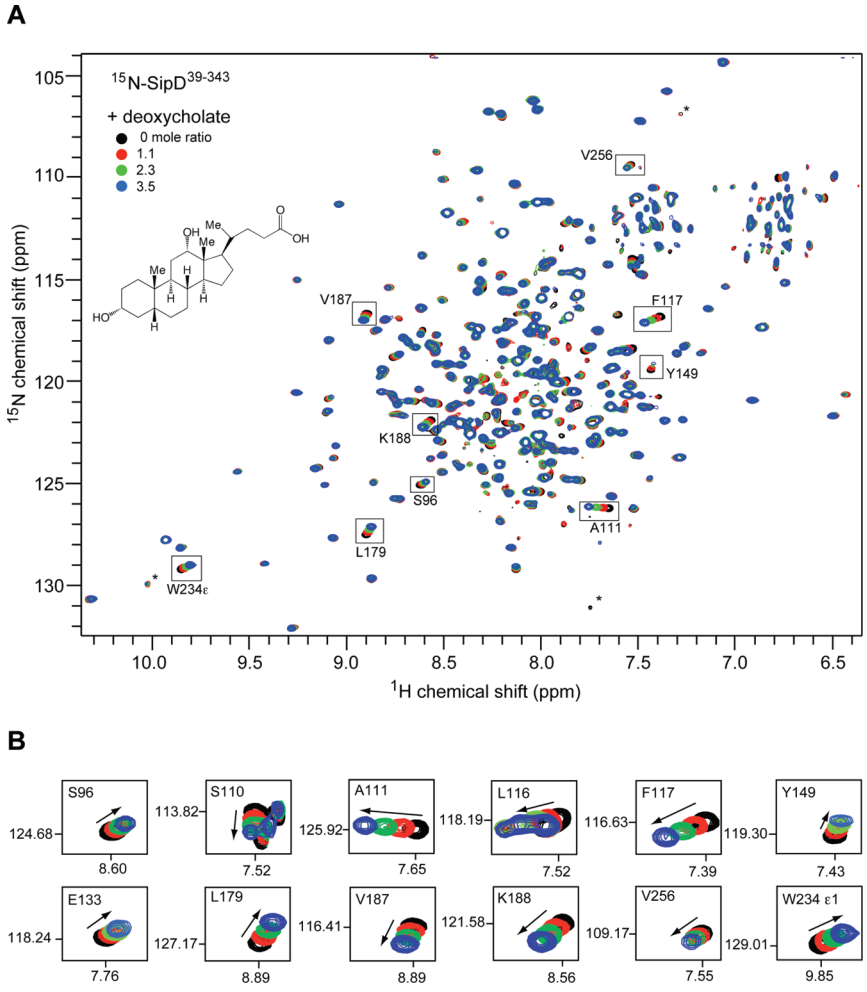

FIGURE 1: (A) Overlay of four 2D ^{1}H−^{15}N TROSY spectra of ^{15}N-labeled SipD$^{39-343}$ with increasing amounts of deoxycholate. Some of the assignments are indicated as well as the noise peaks (*). (B) Expanded regions of the 2D ^{1}H−^{15}N TROSY spectra for specific residues that showed chemical shift changes with deoxycholate (arrows indicate the direction of the chemical shift change). Similar NMR titration data for SipD$^{39-343}$ with taurodeoxycholate (Figure S7), chenodeoxycholate (Figure S8), and cholate hydrate (Figure S9) are shown in the Supporting Information.

The cell lysate was centrifuged (18200*g*, 10 min, 4 °C), and $^{1}/_{10}$ volume of 1% polyethyleneimine (pH 8) was added to the supernatant to precipitate the nucleic acids and then centrifuged (18200*g*, 10 min, 4 °C). The supernatant was loaded onto a 5 mL Ni^{2+}-affinity column (Sigma), washed with 35 mL of binding buffer, and eluted in 1 mL fractions with a total of 15 mL of elution buffer (250 mM imidazole, 500 mM NaCl, 20 mM Tris, pH 8.0). Fractions containing the GB1-SipD$^{39-343}$ fusion protein were combined (into a total volume of 20 mL) and dialyzed overnight at room temperature in 1 L of buffer (50 mM Tris-HCl, 0.5 mM EDTA, 1 mM DTT, 20 mM NaCl, pH 8) in the presence of 50 μL of 0.07 mM recombinant TEV protease that was purified as described (*12*). The digest was loaded onto a 5 mL Ni^{2+}-affinity column, which retained the GB1 tag and eluted SipD$^{39-343}$. Purified SipD$^{39-343}$ was dialyzed in buffer (10 mM sodium phosphate, pH 6.5, and 10 mM NaCl) and concentrated using Amicon Ultra 3K (Millipore), and protein concentration was determined by UV absorbance at 280 nm.

Amino Acid Specific Labeling. In total, eight ^{15}N-amino acid-specifically labeled SipD$^{39-343}$ were prepared using ^{15}N-labeled Leu, Val, Ile, Ala, Phe, Tyr, Met, and Lys. To label SipD$^{39-343}$ with [^{15}N]Leu, for example, *E. coli* BL21(DE3) DNAY harboring the SipD$^{39-343}$ expression plasmid was grown in 1 L of LB medium overnight at 37 °C. The cells were harvested by centrifugation and resuspended in 500 mL of M9 minimal medium supplemented with 125 mg/L [^{15}N]Leu (Isotec) and 600 mg/L of the rest of the 19 unlabeled amino acids. The cells were grown at 37 °C for ~45 min until $A_{600} \sim 0.8$, induced with 1 mM IPTG, and cell growth was continued at 37 °C for 4 h before harvest. Protein was purified as described above.

Mutagenesis of Tryptophan Residues. To assign the side chain resonances of the four tryptophan residues in SipD (W135, W177, W234, and W290), each tryptophan was mutated into tyrosine by the Stratagene QuickChange method. Recombinant ^{15}N-labeled SipD$^{39-343}$ with point mutation W135Y, W177Y, W234Y, or W290Y was expressed and purified as described above.

NMR Spectroscopy. NMR data were acquired at 30 °C on a Bruker Avance 800 MHz spectrometer equipped with a cryogenic triple-resonance probe, processed using NMRPipe (*13*), and analyzed using NMRView (*14*). Proteins were dissolved in NMR buffer (10 mM sodium phosphate, pH 6.5, 10 mM NaCl, and 10% D_2O). For backbone assignments, 0.5 mM perdeuterated ^{15}N,^{13}C-SipD$^{39-343}$ was used to acquire 2D ^{1}H−^{15}N TROSY-HSQC (*15*), 3D TROSY-HNCA (*16*), 3D TROSY-HNCACB (*17*), 3D TROSY-HNCO (*17*), and 3D TROSY-HN(CA)CO (*17*). In addition, 2D ^{1}H−^{15}N TROSY-HSQC (*15*) was acquired using 0.3−0.6 mM ^{15}N-amino acid-labeled

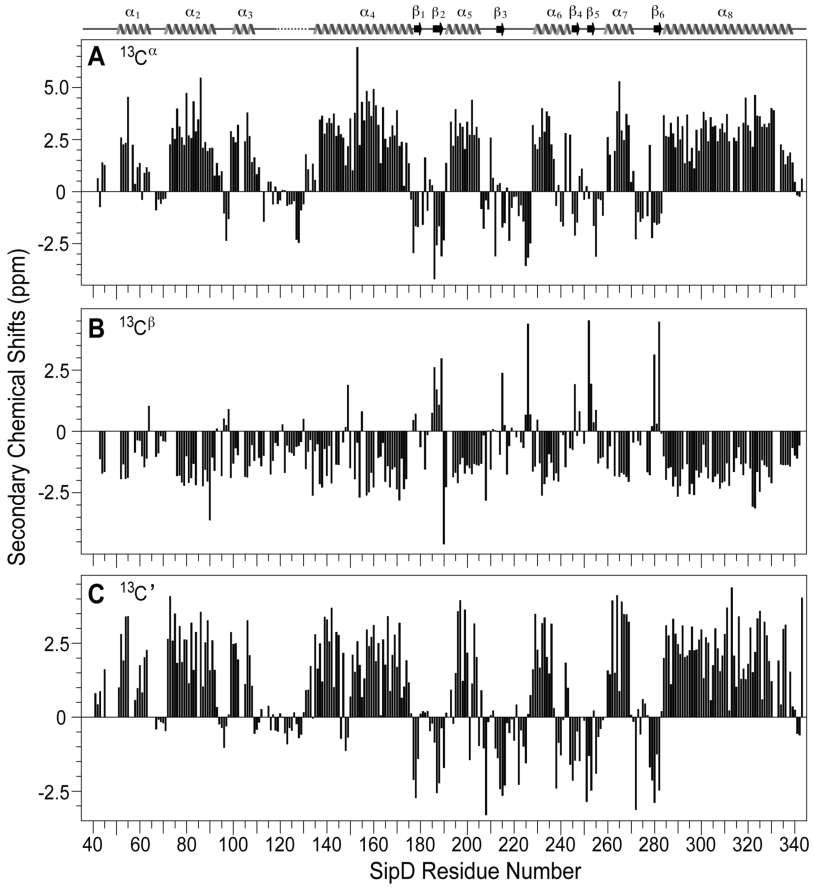

FIGURE 2: Secondary structures of SipD$^{39-343}$ based on the (A) C^{α}, (B) C^{β}, and (C) C′ secondary NMR chemical shifts. The secondary structures of the SipD$^{39-343}$ crystal are also shown and are denoted by arrow (β strand), wavy line (helix), solid line (loop), and broken line (disordered loop). Residues 118−133 lacked electron density in the SipD$^{39-343}$ crystal.

SipD$^{39-343}$. Tryptophan side chains were assigned by acquiring 2D $^{1}H-^{15}N$ HSQC or 2D $^{1}H-^{15}N$ TROSY-HSQC (*15*) using ^{15}N-labeled SipD$^{39-343}$ W135Y, W177Y, W234Y, and W290Y. For NMR chemical shift mapping, 2D $^{1}H-^{15}N$ TROSY-HSQC (*15*) spectra were acquired using ^{15}N-labeled SipD$^{39-343}$ that was titrated with varying amounts of deoxycholate (Amresco), chenodeoxycholate (Sigma), taurodeoxycholate (Sigma), or cholate hydrate (Sigma). NMR samples for chemical shift mapping were prepared as follows: 0.6 mM ^{15}N-SipD$^{39-343}$ was dialyzed overnight in 1 L of NMR buffer containing increasing concentrations of deoxycholate (0, 0.7, 1.4, or 2.1 mM) or chenodeoxycholate (0.0, 0.3, 0.6, 1.3, or 2.6 mM) and 0.7 mM ^{15}N-SipD$^{39-343}$ in NMR buffer with taurodeoxycholate (0.0, 0.3, 0.7, 1.3, or 2.6 mM) or cholate hydrate (0.0, 0.3, 0.7, 1.3, or 2.6 mM).

RESULTS

Protein Expression and Purification. Full-length SipD yielded poor NMR spectra (Figure S1) and was not amenable for NMR characterization. However, the crystal structures of BipD (*11*, *18*) and IpaD (*11*) showed that the N-terminal 29−38 residues were disordered and these proteins were predominantly α-helical in secondary structure. Thus, the N-terminal 38 residues of SipD were truncated, forming the SipD$^{39-343}$ construct used in this study. Recombinant SipD$^{39-343}$ was overexpressed as a fusion protein with the GB1 domain, purified by Ni^{2+}-affinity chromatography, and digested with TEV protease to remove the fusion tag. The circular dichroism (CD) spectra of full-length SipD and SipD$^{39-343}$ were both indicative of highly α-helical proteins (Figure S2). Further, the CD thermal denaturation curves for full-length SipD and SipD$^{39-343}$ (Figure S2) were similar in pattern and showed two transition temperatures at 59 and 75 °C. Thus, CD spectroscopy indicated that SipD$^{39-343}$ retained the core structured domain of SipD. In contrast to full-length SipD, the truncated SipD$^{39-343}$ yielded well-dispersed NMR spectra (Figure 1 and Figure S1C), which allowed further NMR characterization.

NMR Assignment of SipD$^{39-343}$. The backbone resonances of SipD$^{39-343}$ (305 residues) were assigned using perdeuteration, TROSY NMR (Figure S3), and ^{15}N-amino acid-specific labeling (Figure S4). The backbone amides of 274 residues, or 93% of 295 nonproline residues in SipD$^{39-343}$, were assigned. The remaining 7% of backbone amides that could not be assigned were due to peak overlap or peak broadening, and these residues were Arg (41), Leu (48), Thr (65), Glu (103), His (40 and 56), Gln (57 and 262), Asn (72 and 104), and Ser (47, 49, 86, 143, 243, 250, 313, 317, 332, and 333). Nevertheless, nearly complete assignment of the backbone amides allowed the assignment of 93% of the C^{α}, C^{β}, and C′ resonances of SipD$^{39-343}$. The secondary C^{α}, C^{β}, and C′ chemical shifts of SipD$^{39-343}$ (Figure 2) showed a predominantly α-helical protein with several short β strands, which correlated well with the secondary structures of BipD (*11*, *18*) and IpaD (*11*). The chemical shifts suggested that the three-dimensional structure of SipD in solution will be similar to that of the crystal structures of BipD (*11*, *18*) and IpaD (*11*). Indeed, our 1.9 Å resolution crystal structure of SipD$^{39-343}$ (to be reported elsewhere) showed similar secondary structures as

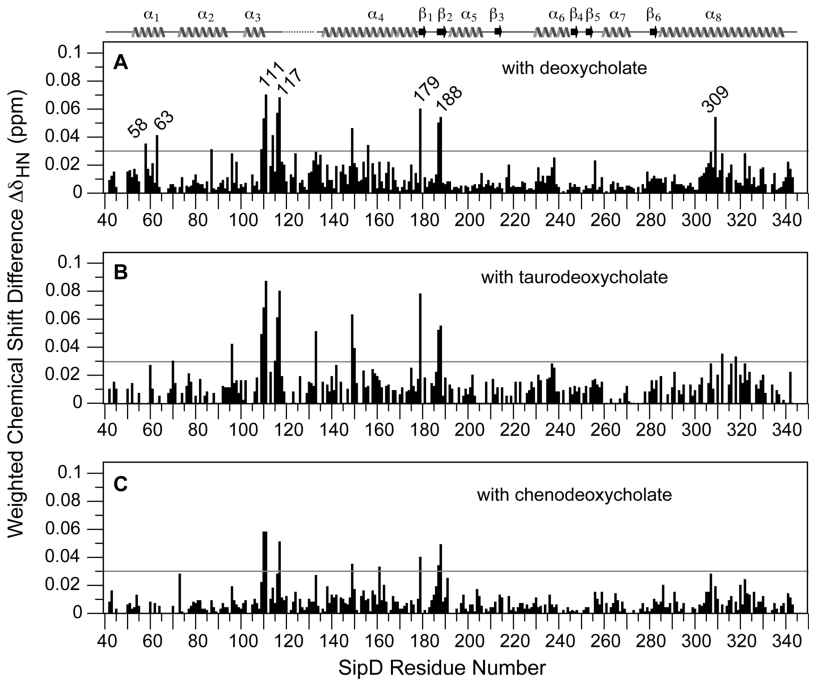

FIGURE 3: Weighted chemical shift difference ($\Delta\delta_{HN}$) of the ^1H and ^{15}N resonances of $SipD^{39-343}$ when titrated with (A) deoxycholate, (B) taurodeoxycholate, and (C) chenodeoxycholate ($\Delta\delta_{HN} = [^1/_2(\delta_H^2 + {}^1/_{25}\delta_N^2)]^{1/2}$ (*25*)). The ^1H and ^{15}N chemical shifts were extracted from the 2D $^1H-^{15}N$ TROSY spectra of the free protein and the protein with the highest molar ratios of titrants at (A) 3.5, (B) 3.7, and (C) 4.3, respectively. For the deoxycholate titration (A), the average $\Delta\delta_{HN}$ for all residues was 0.011 ppm with a standard deviation (σ) of 0.011 ppm. Thus, $\Delta\delta_{HN}$ values above 3σ (or 0.03 ppm, indicated by a horizontal line) were deemed significant. Horizontal lines at $\Delta\delta_{HN}$ 0.03 ppm in (B) and (C) were drawn for comparison with (A).

indicated by the C^{α}, C^{β}, and C′ chemical shifts. Additionally, our SipD crystal structure showed a similar pattern of secondary structures with the IpaD crystal structure (Figure S5), indicating that SipD and IpaD are structurally similar. However, in our $SipD^{39-343}$ crystal structure, residues 118−133, which connect the N-terminal domain with the central coiled coil, lacked electron density and were disordered in the $SipD^{39-343}$ crystal. To assign the tryptophan side chains, the four tryptophan residues (W135, W177, W234, and W290) were each mutated into a tyrosine residue. Proton−nitrogen correlation spectra showed that the tryptophan to tyrosine point mutants were folded, which allowed the assignment of the tryptophan residues in SipD (Figure S6).

NMR Titrations of $SipD^{39-343}$ with Bile Salts. We used NMR chemical shift mapping to investigate the SipD interaction with bile salts deoxycholate, taurodeoxycholate, chenodeoxycholate, and cholate hydrate. ^{15}N-Labeled $SipD^{39-343}$ was dialyzed in buffer with increasing amounts of bile salts, and 2D $^1H-^{15}N$ TROSY spectra were acquired. The protein−bile salt molar ratios used in the NMR titrations were limited by the critical micelle concentrations of deoxycholate (5 mM) (*19*), taurodeoxycholate (2.5 mM) (*20*), and chenodeoxycholate (7 mM) (*19*) (in contrast, the critical micelle concentration of cholate hydrate is 18 mM (*19*)). $SipD^{39-343}$ titrated with deoxycholate (Figure 1), taurodeoxycholate (Figure S7), and chenodeoxycholate (Figure S8) showed many residues with chemical shift perturbations with increasing amounts of bile salts, whereas titration with cholate hydrate (Figure S9) showed only minor chemical shift changes for one residue (L179) and generally no chemical shift perturbation for the rest of $SipD^{39-343}$. Thus, NMR titrations suggested specific interaction of $SipD^{39-343}$ with the deoxycholate (Figure 1), taurodeoxycholate (Figure S7), and chenodeoxycholate (Figure S8) but not with cholate hydrate (Figure S9). Further, the interactions were in the fast-exchange NMR time scale as indicated by the progressive changes in the $SipD^{39-343}$ peak positions with increasing amounts of deoxycholate (Figure 1), taurodeoxycholate (Figure S7), and chenodeoxycholate (Figure S8).

We identified all of the backbone amides and the tryptophan side chain of $SipD^{39-343}$ that were perturbed by deoxycholate, taurodeoxycholate, and chenodeoxycholate. In the presence of deoxycholate, the $SipD^{39-343}$ residues that showed the largest chemical shift perturbations (with $\Delta\delta_{HN} > 0.05$) were S110, A111, L116, F117, Y149, L179, V187, K188, and T309 (Figure 3A). Residues that showed significant chemical shift perturbations (with $\Delta\delta_{HN}$ between 0.03 and 0.05) were A58, Q63, L87, and F109 (Figure 3A). Taurodeoxycholate strongly perturbed the same residues (with $\Delta\delta_{HN} > 0.05$) as deoxycholate in addition to E133 (Figure 3B). For taurodeoxycholate, residues that showed significant chemical shift perturbations (with $\Delta\delta_{HN}$ between 0.03 and 0.05) were E70, S96, F109, A115, L150, Y312, and L318 (Figure 3B). Compared to deoxycholate and taurodeoxycholate, chenodeoxycholate had an overall smaller effect on the chemical shifts of SipD (Figure 3C). For chenodeoxycholate, the strongest perturbations (having $\Delta\delta_{HN} > 0.05$) occurred in residues S110, A111, and F117, with significant perturbations (having $\Delta\delta_{HN}$ between 0.03 and 0.05) in residues Y149, T161, L179, V187, and K188. Chenodeoxycholate perturbed generally the same subset of residues perturbed by deoxycholate and taurodeoxycholate. Regarding the tryptophan side chain, both deoxycholate (Figure 1B) and taurodeoxycholate (Figure S7B) perturbed the W234 side chain whereas chenodeoxycholate (Figure S8B) did not.

A majority of the residues that were strongly perturbed by deoxycholate, taurodeoxycholate, and chenodeoxycholate were located on a 23-residue loop between residues 110 and 134, which connects the N-terminal helix α_1, α_2, and α_3 with the long central

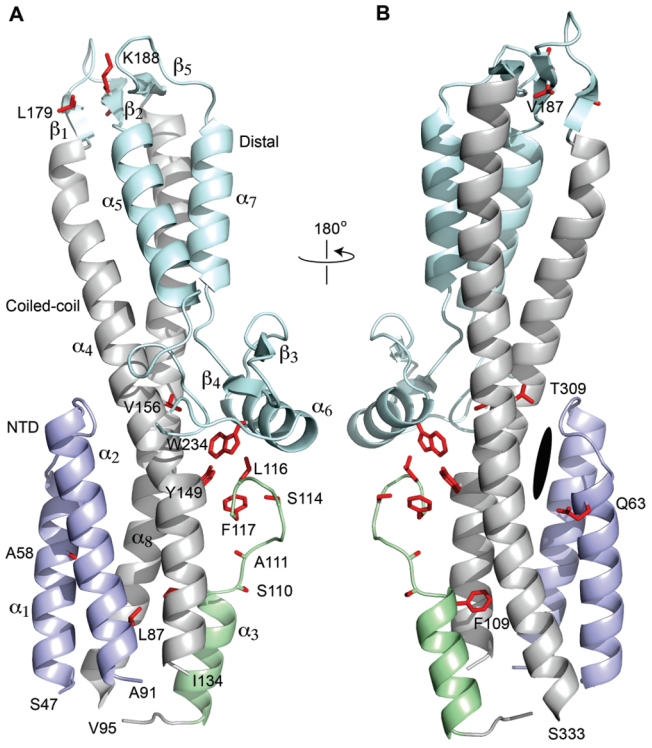

FIGURE 4: Ribbon representation of the crystal structure of SipD$^{39-343}$ (to be reported elsewhere). The side chains of residues that showed significant chemical shift perturbation ($\Delta\delta_{HN} > 0.03$) with deoxycholate were colored red (legend: α, α-helix; β, β strand; dark oval represents the equivalent region in IpaD that was predicted by computer docking to be deoxycholate binding site in IpaD (*7*)). The various regions of SipD were colored as follows: N-terminal helix α_1 and α_2 (light blue), helix α_3 and loop 110−117 (light green), the central coiled coil formed by helix α_4 and α_8 (gray), and the rest of SipD (pale cyan).

coiled coil of SipD (Figure 4). Another subset of residues perturbed by bile salts (residues L179, V187, and K188) was located on β strands β_1 and β_2 on the far end of the central coiled coil and away from loop 110−134 (Figure 4). The N-terminal helix α_1 and α_2 also showed chemical shift perturbations with deoxycholate (residues A58, Q63, and L87) and with taurodeoxycholate (residues E70 and S96), albeit with lesser $\Delta\delta_{HN}$ values compared to loop 110−134 and β strands β_1 and β_2.

DISCUSSION

The major significance of this work is the NMR identification of SipD residues that were perturbed by bile salts (Figure 1, Figures S7 and S8). This was made possible by our NMR assignment of the backbone resonances of SipD (Figure 2). To date, no other tip protein has been assigned by NMR, and this is due to the challenge posed by NMR studies of the tip proteins. SipD, IpaD, and BipD have 343, 332, and 310 residues, respectively. Further, these proteins were soluble only in the submillimolar range, aggregated in NMR solution conditions at high concentrations, and showed poor quality NMR spectra that were unsuitable for NMR characterization. The SipD N-terminal 38 residues, which were expected to be disordered based on structural homology with BipD (*11*, *18*) and IpaD (*11*), decreased the quality of NMR data of full-length SipD (Figure S1). A truncated construct, SipD$^{39-343}$, retained the core structure of SipD (Figure S2) and showed the best quality NMR spectra (Figure S1). Perdeuteration, TROSY (Figure S3), and amino acid-specific labeling (Figure S4) were used to obtain nearly complete backbone assignments for SipD$^{39-343}$. All of the SipD$^{39-343}$ backbone amide peaks that showed chemical shift perturbation with bile salts were assigned (Figure 1, Figures S7 and S8). In addition, the tryptophan side chain peaks of SipD (Figure S6), one of which was perturbed by deoxycholate and taurodeoxycholate, were also assigned.

Another major finding of this work is that the bile salt binding site in SipD obtained from NMR chemical shift mapping is inconsistent with the published model of IpaD−deoxycholate interaction (*7*). Using the computer program AutoDock, Stensrud et al. (*7*) reported a model of the IpaD−deoxycholate complex where deoxycholate binds in a pocket at the interface of the IpaD N-terminal region (equivalent to helix α_1 and α_2 of SipD; see Figure 4) and the long central coiled coil (equivalent to helix α_4 and α_8 of SipD) (Figure 4). If the model of the IpaD−deoxycholate interaction is applied to SipD, the N-terminal helix α_1 and α_2 of SipD (residues 47−91) and the middle part of the coiled coil (helix α_4 and α_8 facing helix α_1 and α_2) would be expected to show relatively the strongest chemical shift perturbations with deoxycholate. However, in our NMR titrations, the N-terminal helix α_1 and α_2 of SipD did not show large chemical shift perturbations with deoxycholate (Figure 3). The helix α_1 and α_2 residues (A58, Q63, and L87) that were perturbed by deoxycholate showed relatively smaller chemical shift perturbations compared to residues that showed the largest chemical shift perturbations (Figure 3). And in helix α_8, only one residue (T309) showed chemical shift perturbation above the threshold of significance (at $\Delta\delta_{HN} = 0.03$). The relatively smaller chemical shift perturbations and the paucity of residues affected lead us to conclude that helix α_1, α_2, and α_8 are not the primary binding sites for deoxycholate in SipD. Instead, for deoxycholate, taurodeoxychoate, and chenodeoxycholate, the strongest chemical shift perturbations occurred in loop 110−134 (Figures 3 and 4), which connects the N-terminal region (helix α_1−α_3) to the central coiled coil (helix α_4 and α_8). Our NMR results suggest that, in SipD, loop 110−134 is most likely involved in interaction with bile salts. Residues L179, V187, and K188 located on β strands β_1 and β_2 (Figure 4) also showed consistently significant chemical shift perturbations (Figure 3); however, these residues are far away from loop 110−134 (Figure 4). Thus, the chemical shift perturbation of L179, V187, and K188 is possibly due to nonspecific interaction with bile salts. On the basis of our chemical shift mapping, we conclude that SipD binds bile salts in a different manner as predicted for IpaD (*7*) despite strong structural similarity between IpaD and SipD (with C^{α} rmsd of 1.4 Å) (Figure S5).

We propose that the difference in the interaction between IpaD and SipD to bile salts reflects the differing responses of *Shigella* and *Salmonella* T3SS to bile salts. Bile salts activate the *Shigella* T3SS (*7*, *8*), whereas they repress the *Salmonella* T3SS (*9*). In *Salmonella*, bile salts repress the transcription of T3SS genes and reduce the secretion of T3SS effectors (*9*, *10*, *21*). The precise target of bile salts *vis-à-vis* T3SS transcriptional regulation is currently unknown (*9*, *10*). Bile salts do not interact directly with any of the T3SS transcriptional regulators (HilA and SirC) (*9*). Prouty and Gunn (*9*) hypothesized that bile salts enter the T3SS regulatory pathway through the two-component system SirA-BarA (which regulates HilA and SirC) or some unknown factor that affects the activity of SirA-BarA. On the other hand, others have shown recently that IpaD is present at the tip of the *Shigella* needle prior to contact with eukaryotic cells (*3*). In the presence of

bile salts, bile salts interact with IpaD and trigger the release of IpaB (*8*), a protein involved in the assembly of the translocon (a membrane spanning structure that punctures a hole in the eukaryotic cell membrane to allow the passage of bacterial proteins). Similarly in *Salmonella*, Lara-Tejero and Galan (*22*) have shown that SipD is present on the bacterial surface before contact with eukaryotic cells, and upon contact with eukaryotic cells, the translocator proteins SipB and SipC are released. Thus, in *Shigella* and *Salmonella*, there is a period when IpaD and SipD are present at the tip of the needle (*3*, *8*, *22*) when they could act as environmental sensors by interacting directly with bile salts. Our results, together with the results of Stensrud et al. (*7*), suggest a model of tip protein−bile salt interaction where IpaD and SipD have different binding sites for bile salts. One site (the IpaD site) results to activation of the T3SS by allowing the assembly of the translocon, and another site (the SipD site) results to inactivation of the T3SS.

Although the use of truncated SipD facilitated the NMR studies reported here, it also prevented the determination of the role of the SipD N-terminal 38 residues with respect to bile salt interaction. It is expected, however, that the main function of the N-terminal region is as a type III secretion signal (*23*, *24*) rather than for bile−salt interaction. Another limitation of the current work is that the NMR method used here could not determine the K_d of the SipD−bile salt interaction, which is needed for functional studies of SipD−bile salt interaction. The reason for this is that the chemical shift changes did not reach saturation during the titration. Increasing the amount of bile salts was not possible because of the limitation imposed by the millimolar CMCs of bile salts and the requirement for submillimolar amounts of $Sipd^{39-343}$ for NMR. Because of the poor quality of the NMR spectrum of the full-length SipD (Figure S1B), it was also not possible to use the full-length SipD in binding studies by NMR methods. Isothermal calorimetry also failed to determine the K_d because the heat generated by (full-length and truncated) SipD upon titration with bile salts was lower than the heat generated by micelle formation of bile salts (*19*). Thus, a more sensitive method such as fluorescence spectroscopy, which was successfully used in studies of IpaD−bile salt interaction (*7*), would have to be used to determine the K_d of SipD−bile salt interaction.

In summary, we have used NMR methods to investigate the interaction of SipD with bile salts and found that the interaction is different from what was predicted for IpaD−bile salt interaction. The differing response of SipD and IpaD to bile salts is most likely related to the opposing responses of *Shigella* and *Salmonella* to bile salts. Our results presented herein contribute to our understanding of the molecular interactions involved in type III secretion.

ACKNOWLEDGMENT

We are grateful to Dr. Gianluigi Veglia (University of Minnesota) for assistance in specific labeling, to Chet Egan for CD spectroscopy, and to Asokan Anbanandam for NMR spectroscopy.

SUPPORTING INFORMATION AVAILABLE

HSQC optimization of SipD constructs (Figure S1); CD spectroscopy of SipD (Figure S2); 3D NMR data used in the backbone assignments of SipD (Figure S3); amino acid specific labeling of SipD (Figure S4); alignment of secondary structures of IpaD and SipD (Figure S5); assignment of tryptophan side chain by mutagenesis (Figure S6); titration of SipD with taurodeoxycholate (Figure S7), chenodeoxycholate (Figure S8), and cholate hydrate (Figure S9). This material is available free of charge via the Internet at http://pubs.acs.org.

REFERENCES

1. Cornelis, G. R. (2006) The type III secretion injectisome. *Nat. Rev. Microbiol. 4*, 811–825.
2. Mueller, C. A., Broz, P., Muller, S. A., Ringler, P., Erne-Brand, F., Sorg, I., Kuhn, M., Engel, A., and Cornelis, G. R. (2005) The V-antigen of *Yersinia* forms a distinct structure at the tip of injectisome needles. *Science 310*, 674–676.
3. Espina, M., Olive, A. J., Kenjale, R., Moore, D. S., Ausar, S. F., Kaminski, R. W., Oaks, E. V., Middaugh, C. R., Picking, W. D., and Picking, W. L. (2006) IpaD localizes to the tip of the type III secretion system needle of *Shigella flexneri*. *Infect. Immun. 74*, 4391–4400.
4. Picking, W. L., Nishioka, H., Hearn, P. D., Baxter, M. A., Harrington, A. T., Blocker, A., and Picking, W. D. (2005) IpaD of *Shigella flexneri* is independently required for regulation of Ipa protein secretion and efficient insertion of IpaB and IpaC into host membranes. *Infect. Immun. 73*, 1432–1440.
5. Stevens, M. P., Haque, A., Atkins, T., Hill, J., Wood, M. W., Easton, A., Nelson, M., Underwood-Fowler, C., Titball, R. W., Bancroft, G. J., and Galyov, E. E. (2004) Attenuated virulence and protective efficacy of a *Burkholderia pseudomallei bsa* type III secretion mutant in murine models of melioidosis. *Microbiology 150*, 2669–2676.
6. Kaniga, K., Trollinger, D., and Galan, J. E. (1995) Identification of two targets of the type III protein secretion system encoded by the inv and spa loci of *Salmonella typhimurium* that have homology to the *Shigella* IpaD and IpaA proteins. *J. Bacteriol. 177*, 7078–7085.
7. Stensrud, K. F., Adam, P. R., La Mar, C. D., Olive, A. J., Lushington, G. H., Sudharsan, R., Shelton, N. L., Givens, R. S., Picking, W. L., and Picking, W. D. (2008) Deoxycholate interacts with IpaD of *Shigella flexneri* in inducing the recruitment of IpaB to the type III secretion apparatus needle tip. *J. Biol. Chem. 283*, 18646–18654.
8. Olive, A. J., Kenjale, R., Espina, M., Moore, D. S., Picking, W. L., and Picking, W. D. (2007) Bile salts stimulate recruitment of IpaB to the *Shigella flexneri* surface, where it colocalizes with IpaD at the tip of the type III secretion needle. *Infect. Immun. 75*, 2626–2629.
9. Prouty, A. M., and Gunn, J. S. (2000) *Salmonella enterica* serovar typhimurium invasion is repressed in the presence of bile. *Infect. Immun. 68*, 6763–6769.
10. Prouty, A. M., Brodsky, I. E., Manos, J., Belas, R., Falkow, S., and Gunn, J. S. (2004) Transcriptional regulation of *Salmonella enterica* serovar Typhimurium genes by bile. *FEMS Immunol. Med. Microbiol. 41*, 177–185.
11. Johnson, S., Roversi, P., Espina, M., Olive, A., Deane, J. E., Birket, S., Field, T., Picking, W. D., Blocker, A. J., Galyov, E. E., Picking, W. L., and Lea, S. M. (2007) Self-chaperoning of the type III secretion system needle tip proteins IpaD and BipD. *J. Biol. Chem. 282*, 4035–4044.
12. Geisbrecht, B. V., Bouyain, S., and Pop, M. (2006) An optimized system for expression and purification of secreted bacterial proteins. *Protein Expression Purif. 46*, 23–32.
13. Delaglio, F., Grzesiek, S., Vuister, G. W., Zhu, G., Pfeifer, J., and Bax, A. (1995) NMRPipe: a multidimensional spectral processing system based on UNIX pipes. *J. Biomol. NMR 6*, 277–293.
14. Johnson, B. A. (2004) Using NMRView to visualize and analyze the NMR spectra of macromolecules. *Methods Mol. Biol. 278*, 313–352.
15. Czisch, M., and Boelens, R. (1998) Sensitivity enhancement in the TROSY experiment. *J. Magn. Reson. 134*, 158–160.
16. Salzmann, M., Pervushin, K., Wider, G., Senn, H., and Wuthrich, K. (1998) TROSY in triple-resonance experiments: new perspectives for sequential NMR assignment of large proteins. *Proc. Natl. Acad. Sci. U.S.A. 95*, 13585–13590.
17. Salzmann, M., Wider, G., Pervushin, K., Senn, H., and Wuthrich, K. (1999) TROSY-type triple-resonance experiments for sequential NMR assignments of large proteins. *J. Am. Chem. Soc. 121*, 844–848.
18. Erskine, P. T., Knight, M. J., Ruaux, A., Mikolajek, H., Sang, N. W., Withers, J., Gill, R., Wood, S. P., Wood, M., Fox, G. C., and Cooper, J. B. (2006) High resolution structure of BipD: an invasion protein associated with the type III secretion system of *Burkholderia pseudomallei*. *J. Mol. Biol. 363*, 125–136.
19. Simonovic, B. R., and Momirovic, M. (1997) Determination of critical micelle concentration of bile acid salts by micro-calorimetric titration. *Mikrochim. Acta 127*, 101–104.

20. DeLong, L. J., and Nichols, J. W. (1996) Time-resolved fluorescence anisotropy of fluorescent-labeled lysophospholipid and taurodeoxycholate aggregates. *Biophys. J. 70*, 1466–1471.
21. van Velkinburgh, J. C., and Gunn, J. S. (1999) PhoP-PhoQ-regulated loci are required for enhanced bile resistance in *Salmonella* spp.. *Infect. Immun. 67*, 1614–1622.
22. Lara-Tejero, M., and Galan, J. E. (2009) *Salmonella enterica* serovar typhimurium pathogenicity island 1-encoded type III secretion system translocases mediate intimate attachment to nonphagocytic cells. *Infect. Immun. 77*, 2635–2642.
23. Karavolos, M. H., Roe, A. J., Wilson, M., Henderson, J., Lee, J. J., Gally, D. L., and Khan, C. M. (2005) Type III secretion of the *Salmonella* effector protein SopE is mediated via an N-terminal amino acid signal and not an mRNA sequence. *J. Bacteriol. 187*, 1559–1567.
24. Arnold, R., Brandmaier, S., Kleine, F., Tischler, P., Heinz, E., Behrens, S., Niinikoski, A., Mewes, H. W., Horn, M., and Rattei, T. (2009) Sequence-based prediction of type III secreted proteins. *PLoS Pathog. 5*, e1000376.
25. Grzesiek, S., Bax, A., Clore, G. M., Gronenborn, A. M., Hu, J. S., Kaufman, J., Palmer, I., Stahl, S. J., and Wingfield, P. T. (1996) The solution structure of HIV-1 Nef reveals an unexpected fold and permits delineation of the binding surface for the SH3 domain of Hck tyrosine protein kinase. *Nat. Struct. Biol. 3*, 340–345.